Optics Communications 502 (2022) 127397

Contents lists available at ScienceDirect

Optics Communications

journal homepage: www.elsevier.com/locate/optcom

Defining speckle-based spectral metric from a linear array detector for characterizing the laser focusing spot

Dongbo Che [a,b], Tingfeng Wang [a], Shao Zhang [a,b], Yuanyang Li [a], Yue Han [a,b], Zhan Yu [a,*]

[a] State Key Laboratory of Laser Interaction with Matter, Changchun Institute of Optics, Fine Mechanics and Physics, Chinese Academy of Sciences, Changchun, 130033, China

[b] Center of Materials Science and Optoelectronics Engineering, University of Chinese Academy of Sciences, Beijing, 100049, China

ARTICLE INFO

Keywords:
Speckle
Arrays
Optical sensing and sensors
Scattering
Rough surfaces

ABSTRACT

Speckle modulation in the laser beam projection scenarios such as adaptive optics, remote sensing, and active imaging has been a long-standing challenge that causes intensity fluctuation and further degrades the performance of the system. Speckle statistical characteristics coupled with the feature of the laser beam intensity distribution can be obtained by analyzing the speckle variation through a single point detector or an image sensor. A single point detector has the advantage in high sampling rate but may lose speckle spatial information, while the image sensor has a high spatial resolution but slow sampling rate. In this paper, we defined a dynamic speckle metric based on a linear array detector to estimate the encircled energy of the far-field spot on the diffuse target, which well balanced the trade-off between sampling rate and spatial resolution. The potential of the metric is analyzed using a physics-based speckle simulation and experimental verification. Both results agree with each other, showing that the metrics based on the speckle-field spatiotemporal spectrum analysis are monotonically dependent on the target focused-spot size.

1. Introduction

In laser beam projection scenarios typical of remote sensing, adaptive optics and directed energy applications, a transmitted laser beam propagates through a long-distance toward a remote target, scatters off the target's surface [1], and returns to the transceiver plane, which is referred to as double-pass wave propagation configuration [2]. In the case of cooperative targets, the standard phase conjugate adaptive optics system [3] which uses a Shack-Hartmann wavefront sensor is gradually replaced by the target-in-the-loop (TIL) method which evaluates the far-field *Strehl* ratio by applying trial dither control voltage matrix to the deformable mirror randomly and employing a stochastic parallel gradient descent (SPGD) algorithm to maximize the value of the sensor metric [4]. Besides, a power-in-the-bucket (PIB) metric sensor, placed on the target of interest, is usually utilized to serve as the feedback of the system, ensuring the consistency between the metric signal from the observation plane and the PIB sensor metric. However, the PIB sensor on the target is not always available, especially in a double-pass propagation issue with the uncooperative target. More commonly, the light backscattered from the target is the only decisive criterion of minimizing the size of the hit spot or maximizing the Strehl ratio. In the uncooperative TIL system, the validity and stability of the PIB sensor are compromised by the speckle effects which originate from the turbulence effect, rough target, or their coupling. Direct observation through a telescope [5], on the other hand, is affected by pixelation, making it difficult to monitor very small or jittery spots on the far-field target surface.

The scattered light generated by interference between optical fields from a large number of scatters [6] under coherent light illumination is stochastic and forms a speckle pattern in a far field. The speckle field has become available research because the reflected speckle field not only limits the development of directed energy and adaptive optics techniques but also carries information about the laser beam parameters of the diffuse object. Based on Goodman's ideal Gaussian speckle statistical theory [7], the average speckle size can provide metrics for estimating the laser beam that concentrates on the remote rough target surface. With the study of second and forth order statistics of the received speckle field [8], target-plane beam quality metrics, which include PIB [9], brightness function [10], the clipped speckle intensity auto-correlation [11] and cross-correlation function [12], have been introduced. These dynamic speckles metrics, which are affected by large fluctuations from the signal's stochastic nature and described by a space-time correlation function, require a large number of data sources to improve accuracy. But it is difficult to measure enough data for a slow-moving target or slow-deflecting laser beam in a short time while ensuring accuracy.

In this paper, we proposed a speckle-field based-spectrum metric evaluating method, which can estimate the target focused-spot size. In

* Corresponding author.
E-mail address: yuzhan2425@163.com (Z. Yu).

https://doi.org/10.1016/j.optcom.2021.127397
Received 31 May 2021; Received in revised form 8 August 2021; Accepted 17 August 2021
Available online 24 August 2021

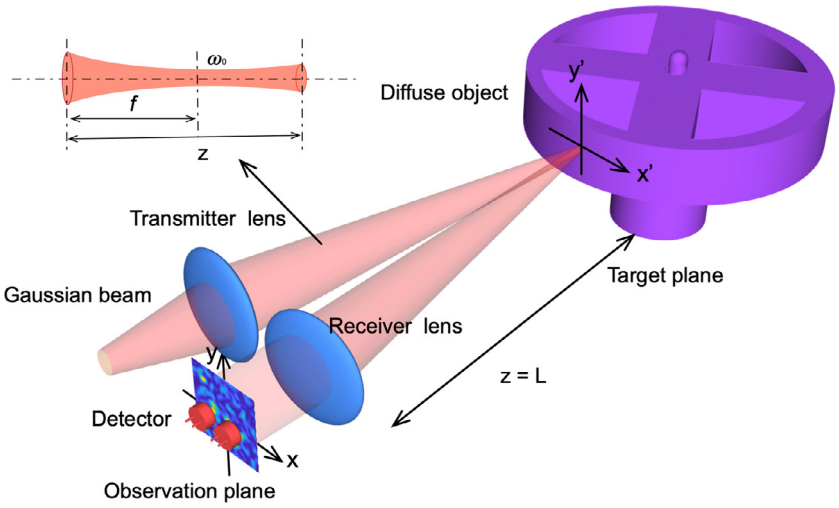

Fig. 1. The coordinate system of dynamic speckle formation geometry. A Gaussian probe beam is directed onto the fast-moving diffuse surface (x', y') or (r', θ), offset by axial displacement $z = L$, while the beam focal plane is located at a distance f from the transmitter lens. Backscattered light is then collected by the receiver lens to form the speckle pattern which is observed in the observation plane (x, y) or (r, α).

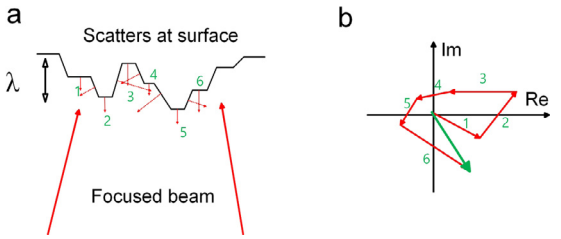

Fig. 2. (a) The surface scatters under illumination experience a random phase modulation due to the optical path difference especially when the rms value of surface height is larger compared to λ. Under this assumption the phasor is uniformly distributed over $[-\pi, +\pi]$. (b) The six randomly phasors shown in (a) may be interpreted as a random walk in complex plane.

Section 2.1, the speckle formation geometry is introduced by the scalar diffraction theory. The characteristics of the speckle are educed by the space-time correlation function in Section 2.2. Section 2.3 details the simulation of the dynamic speckle's time evolution and the methodology on how to obtain the time history of speckle pattern (THSP) from the stacked speckle cube. In Section 2.4, the dependency between speckle metric and beam spot size is analyzed by evaluating the bandwidth of the temporal spectrum and spatial spectrum respectively. Section 3 presents the experimental results to verify the feasibility of the speckle metrics. Finally, the conclusions are given in Section 4.

2. Theoretical work

2.1. Speckle formation geometry

The speckle formation geometry in a TIL system is shown in Fig. 1. In the particular free-space geometry, Fresnel integral based on scalar diffraction theory is utilized to build the model of speckle formation, which represents the value of the complex field at point (r, α) as a sum of many random phasors. Under a Huygens approximation, each phasor can be considered as a spherical wave scattering outward from diffuse scatters with specific magnitude and phase. These wavefronts constructively and destructively interfere at point (r, α), yielding a consequent speckle pattern which can be expressed as a random work in the complex plane shown in Fig. 2b.

The complex field at observation plane $E(r)$ can be mathematically expressed [13]

$$E(r) = \frac{e^{ik}}{i\lambda z} e^{\frac{ikr^2}{2z}} \iint_{-\infty}^{+\infty} E_s(r', \theta) e^{\frac{ikr'^2}{2z}} e^{-\frac{ik}{z}[rr' \cos(\alpha-\theta)]} r' dr' d\theta \tag{1}$$

where λ is the light wavelength and $k = 2\pi/\lambda$ is the wavenumber. Note that Eq. (1) may be interpreted as a Fourier-transformation for the spatial frequency $f_r = r/\lambda z$, which is the foundation of simulation. The backscattered field $E_s(r')$ in Eq. (1) is the product of illumination over the diffuse surface and a phase variation arising from the realization of surface roughness. In most cases, the Gaussian mode coherent beam may be taken as prober and a dynamic deep random phase screen is typically adapted assuming the scattering surface moves in-plane in the r'-direction at speed v. Under these assumptions, the field $E_s(r')$ can be given as

$$E_s(r') = \underbrace{\frac{\omega_0}{\omega} \exp\left[-\left(\frac{1}{\omega^2} + \frac{ik}{2\rho}\right) r'^2 - ik(z-f)\right]}_{\text{Gaussian beam illumination}} \times \underbrace{\exp[i\phi(r' + vt)]}_{\text{surface-induced phase}} \tag{2}$$

where

$$\omega = \omega_0 \left[1 + \frac{(z-f)^2}{a^2}\right]^{1/2} \tag{3}$$

with a Rayleigh length $a = \pi\omega_0^2/\lambda$, is the radius of illuminated beam spot on the scattering surface which is determined by the beam waist (ω_0) and the focal length of the focusing optics (f). And

$$\rho = (z-f)\left[1 + \frac{a^2}{(z-f)^2}\right] \tag{4}$$

is the beam radius of curvature at the incident point. The rough surface-induced phase variation ϕ is realized by an idealization of Gaussian rough surface, called deep random-phase screen, which treats the wavelength of light and the surface height as the function's variable under the assumption that the RMS value of the surface height is relatively larger than the light wavelength. Generally, a white noise process is adopted for the generation of the surface-induced phase variation ϕ which is a uniform random distribution over the interval $[-\pi, +\pi]$, ensuring a fully-developed speckle formation.

2.2. Correlation function of dynamic speckles

Speckle dynamics characterize the variation of the speckle's spatial pattern with respect to time, whose statistical properties are mostly described by the space-time correlation function [13,14]. The normalized

correlation function [13,15] is expressed as

$$\mu_I(\Delta r,\tau)=\frac{\langle \mathbf{I}_1\mathbf{I}_2\rangle}{\langle \mathbf{I}_1\rangle\langle \mathbf{I}_2\rangle}=1+\frac{\left\langle \mathbf{E}_1\mathbf{E}_2^*\right\rangle}{\left(\left\langle |\mathbf{E}_1|^2\right\rangle\left\langle |\mathbf{E}_2|^2\right\rangle\right)^{1/2}} \tag{5}$$

where $\langle \mathbf{I}_1\mathbf{I}_2\rangle=\langle \mathbf{I}(r,t)\mathbf{I}(r+\Delta r,t+\tau)\rangle$ describes the similarity between the light intensity $\mathbf{I}_1$ at time t and the intensity $\mathbf{I}_2$ at time $t+\tau$, $\langle\dots\rangle$ represents an ensemble average.

Substituting Eqs. (1) and (2) into Eq. (5) and calculating the integral formula to get

$$\mu_I(\Delta r,\tau)-1=\exp\left(-\frac{v^2\tau^2}{\omega^2}\right)\exp\left\{-\frac{\left[\Delta r-\left(1+\frac{z}{\rho}\right)v\tau\right]^2}{r_s^2}\right\} \tag{6}$$

where r_s indicates the average radius of the individual speckle lobe, which defines the speckle pattern's correlation length in the observation plane, given by

$$r_s=\frac{\lambda z}{\pi\omega} \tag{7}$$

As the scattering surface gradually deviates from its original position, the micro-scatters contributed to the diffraction process are updated gradually, resulting in that the speckles diverge from the initial pattern with the correlation function becoming less correlated. As indicated in the first term in Eq. (6), the speckle pattern significantly changes only if the scatters are shifted by a large part of beamwidth. Intuitively, once the relative displacement between the scattering surface and laser beam exceeds the beam size, expressed as

$$v\tau>\omega \tag{8}$$

the correlation function drops below e^{-1}, we say that the speckle loses coherence. The spatial correlation properties of the speckle are shown by the second term in Eq. (6), where the value of the correlation function reaches a maximum as the speckle translation length (defined in Ref. [13]) satisfies

$$\Delta r=\left(1+\frac{z}{\rho}\right)\omega \tag{9}$$

Note that the movement of the speckle pattern does not simply reflect the scattering surface motion. Instead, it strongly depends on the coordinate system and optical configuration, which can be fully characterized by the illuminated beam spot ω, offset distance z, and beam radius of curvature ρ.

And the correlation function $\mu(\tau)$ of the speckle-field intensity fluctuation in the receiver area can be defined as

$$\begin{aligned}\mu(\tau)&=\int P\left(\mathrm{r}_1\right)P\left(\mathrm{r}_2\right)\mu_{\delta I}(\Delta\mathrm{r},\tau)\mathrm{d}^2r_1\ \mathrm{d}^2r_2\\&=C\int I_s(\mathrm{r})I_s\left(\mathrm{r}+\mathrm{v}\tau\right)\mathrm{d}^2r\end{aligned} \tag{10}$$

where $P(r)$ is the pupil function of telescope receiver. In the case of a circular aperture with radius a_R, the pupil function can be described as $P(r)=1$ for $|r|\le a_R$, and $P(r)=0$ otherwise. Moreover, $C=M_0[k/(2\pi L)]^4$, $M_0=\int P(r_1)P(r_1+\Delta\mathrm{r})d^2\mathbf{r}$ and the intensity of the target hit spot is $I_s(\mathbf{r})$. So the power spectrum $G_{\delta I}$ of speckle-field is given by

$$\begin{aligned}G_{\delta I}(\varpi)&=\frac{1}{\pi}\int_0^\infty\mu(\tau)\cos(\varpi\tau)d\tau\\&=\frac{C}{\pi}\int_0^\infty\int\cos(\varpi\tau)I_s(\mathbf{r})I_s\left(\mathbf{r}+\mathbf{v}\tau\right)d^2\mathbf{r}d\tau\end{aligned} \tag{11}$$

Correspondingly, the intensity of the target hit spot $I_s(\mathbf{r})$ satisfies a Gaussian distribution $I_s(\mathbf{r})=I\exp\left(-r^2/\omega^2\right)$, the power spectrum $G_{\delta I}(\varpi)$ can be defined as:

$$G_{\delta I}(\varpi)=G_{\delta I}(0)\exp\left[-\frac{\varpi^2}{\left(\varpi_{\delta I}\right)^2}\right] \tag{12}$$

where $\varpi_{\delta I}=v/\omega$ is the characteristic frequency spectrum bandwidth of speckle field, note that the power spectrum bandwidth (cutoff) frequency increases with surface velocity and decreases with the target hit-spot size ω. The characteristic width of the spectrum reveals the size of the target focused spot, this property is the basis for the TIL speckle metrics.

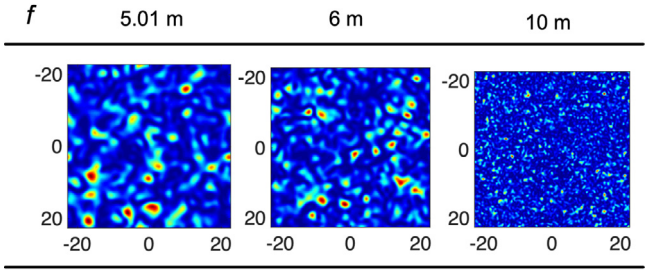

Fig. 3. Speckle pattern generated under different optical configurations. Under the simulation geometry, the transmission distance z is set to be fixed while the focal length of the transmitting lens is changed to achieve a varying focusing state: f = 5.01 m corresponding to a collimated beam, f = 10 m corresponding to a divergent beam.

2.3. Simulation of dynamic speckle

To numerically illustrate the speckle pattern, we straightly simulate the observation plane field $E(r)$ scattered from a fast-moving diffusor according to Eq. (1). First, a deep random phase screen of 15 mm ×15 mm size is discretized into a 256 × 256 pixel grid, whose value is assigned with a uniform distribution between $[-\pi,+\pi]$. And the RMS value of surface height is set to $10^*\lambda$. Then, the phase screen is multiplied by a Gaussian illumination function with a $1/e^2$ diameter (ω_0) of 500 μm, yielding the scattered field $E_s(r')$. The scattered field is finally propagated to the observation plane via a Fourier-transform [16]. As pictured in Fig. 1, a continuous-varying focusing state of the Gaussian beam is realized by varying the value of focal length f with respect to a fixed propagation distance z = 5 m, which results in a varying hit spot size. Three different optical configurations are implemented to demonstrate the dependencies of speckle grain's size on the illumination beam radius, with simulation results shown in Fig. 3. It is agreed with Eq. (7) that the simulated speckle size decreases as the illumination area increases due to the focal plane away from the target.

In order to simulate speckle dynamics, for one-time step iteration, the discretized random phase screen $\phi(r')$ is shifted in the r'-direction by a fixed step offset, which is divided by the variable time step to quantify the speed of moving diffusor. As the cumulative displacement of the phase screen under the illumination increases, the speckle pattern evolves with respect to time. The visualizations of the speckle dynamics corresponding to the configurations shown in Fig. 3 visualize these speckle field evolutions, which describe the speckle boiling, speckle translation and a combination of boiling and translation respectively [17]. These visualized videos provide an intuitive understanding of speckle dynamics why a boiling dominated speckle behavior is observed when the scattering diffusor is near to the laser beam focal plane. These speckle dynamics result from laser beam dithering or surface motion physically but result in temporal intensity fluctuations of the speckle field.

To better demonstrate the 3D Spatio-temporal characteristics of speckles, the varying speckle patterns are stacked to form a speckle cube as shown in Fig. 4a, which represents the evolution of the 256 × 256 speckle pattern during the observation. The x–y plane of the speckle cube (the speckle pattern) only contains the spatial information of the speckle, while the $x-t$ plane of the speckle cube, also called time history of speckle pattern (THSP), implies not only space but also time information. As shown in Fig. 4b, the THSP is obtained by slicing through the center column in the speckle cube. The horizontal length of

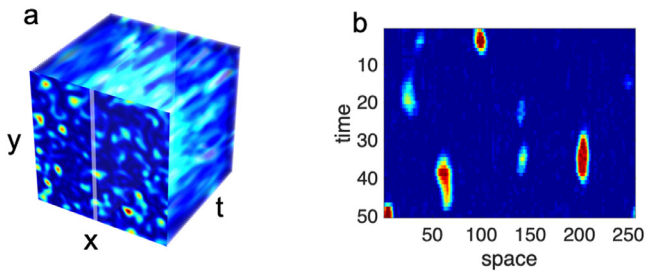

Fig. 4. (a) Speckle cube. (b) Slice through the center column in the speckle cube representing the time history of the speckle pattern (THSP). The horizontal length of the speckle lobe demonstrates the space property in single dimension while the length of speckle lobe in time scale indicates the lifetime of the speckle.

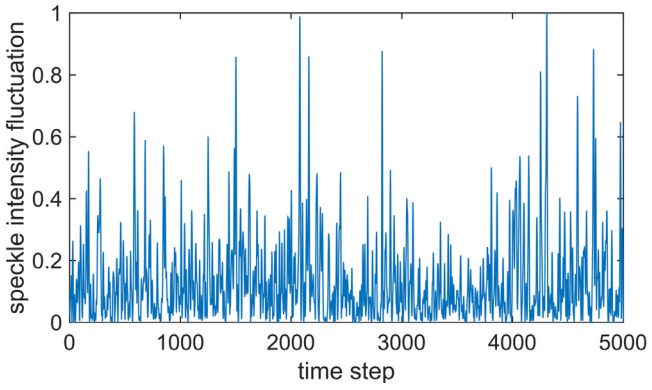

Fig. 5. The normalized speckle-field intensity fluctuation signal is obtained by averaging several columns in Fig. 4b, and the time series is extended to 5000.

the speckle lobe demonstrates the space property in a single dimension while the vertical length of the speckle lobe in time scale indicates the lifetime of the speckle. Therefore, the THSP array processing can effectively cover the Spatio-temporal information of the speckle and can reduce the complexity caused by the cube calculation. In the next section, we will give a methodology on how to extract effective speckle metrics from the obtained THSP to evaluate the beam focus quality and the feasibility of using it as a closed-loop control feedback factor.

2.4. Speckle metrics for beam focusing state based on spectrum analysis

Using Eq. (9), the speckle-field realizations inside non-overlapping areas separated by the speckle translation length Δr can be considered as statistically independent. Sensing of the speckle-field intensity distributions in the receiver areas a_R can be performed by operating in parallel speckle metric sensors such as a line scan camera. And the evolution of speckle-field intensity fluctuation signal obtained by some pixels in the receiver is shown in Fig. 5, which is linked with temporal PIB fluctuations by the Fourier transform relationship. On the other hand, the spatial power spectrum can be obtained by the Fourier transform of the speckle-field spatial intensity fluctuations (the rows in Fig. 4b).

An important property of both correlation function and power spectrum is that it depends on the target focused spot intensity distribution I_r as shown in Eqs. (10) and (12). This property allows one to obtain speckle metrics for monitoring the energy of far-field target hit-spot. Note that the low-frequency spectral components cause large fluctuations in short sampling time T. To reduce the large estimation bias existing in the calculation results, we perform spectral filtering on the signal. Eq. (13) shows the speckle metric J obtained by integrating the power spectrum $G_{\delta I}(\varpi)$ only within one spectral region, where the

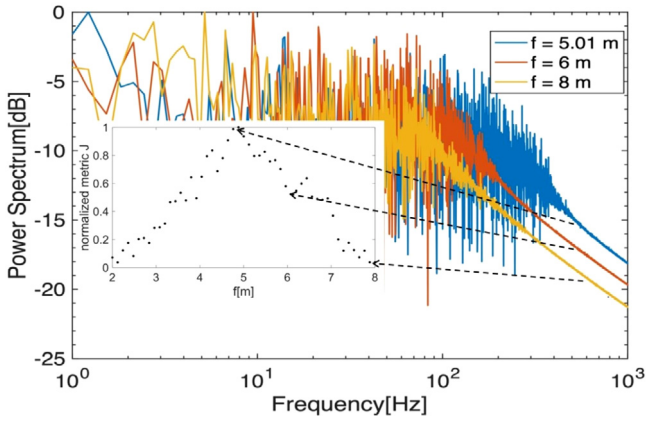

Fig. 6. The power spectrums and the normalized speckle metrics J_{time} are obtained by temporal spectrums. And the target hit-spot size is changed by moving the focal length from 2 m to 8 m with $\Delta f = 0.12$ m. The speckle metrics J_{time} have a maximum at the focal point ($f = 5$ m) corresponding to the smallest possible beam size on the target.

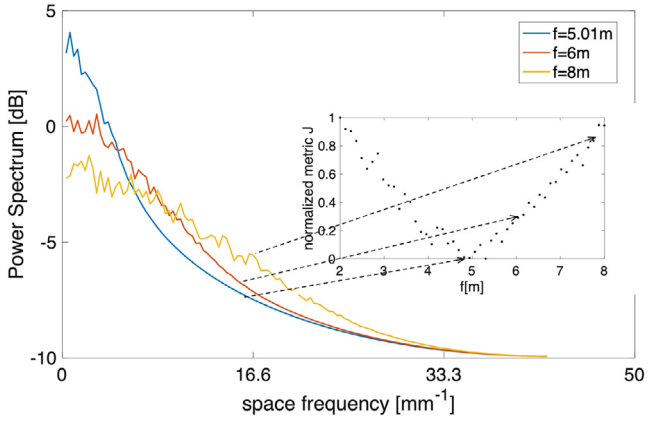

Fig. 7. The power spectrums and normalized speckle metrics J_{space} are obtained by multiple spatial spectrums. The speckle metrics J_{space} have a minimum at the focal point ($f = 5$ m) corresponding to the smallest possible beam size on the target.

accuracy in determining the signal spectral components is high.

$$J = \sum_{i=1}^{n} \beta_i G_{\delta I}\left(\varpi_i, \Delta\right) \tag{13}$$

where $\beta_i = 1/(n-i)$ is the weighting coefficient. And divide the spectrum equally into $(n-1)$ parts. Δ is the width of each spectral band and ϖ_i is the center frequency corresponding to each spectral region. The accuracy of the speckle metric J mainly depends on the weight parameter β_i.

The space and time scales to fulfill the speckle-averaging condition are shown in Table 1. For computing speckle metric J_{time} obtained by space-averaging the temporal power spectrum, the space interval Δr_{space} between temporal spectrums should exceed the speckle translation length Δr, that is $\Delta r_{space} > \left(1 + \frac{z}{\rho}\right)\omega$, to obtain statistically independent speckle pattern realizations. $\Delta\tau$ is the time interval between subsequent measurements, the complete update of surface roughness realizations occurs at the time scale $\tau_s = \omega/v$. And the characteristic time τ_{at} represents the phase distortion change time, which commonly varies from 10^{-1} to 10^{-3} s or even considerably less when tracking fast-moving targets. Correspondingly, the total time required for the speckle metric measurement is $T = N_\tau * \Delta\tau$, where N_τ is the number of instantaneous speckle-field intensity distributions. So the measurement time T need long enough to retrieve the temporal statistical properties ($T \gg \tau_s > \Delta\tau$). On the other hand, the measurement must be less than the characteristic time τ_{at} in an adaptive TIL system,

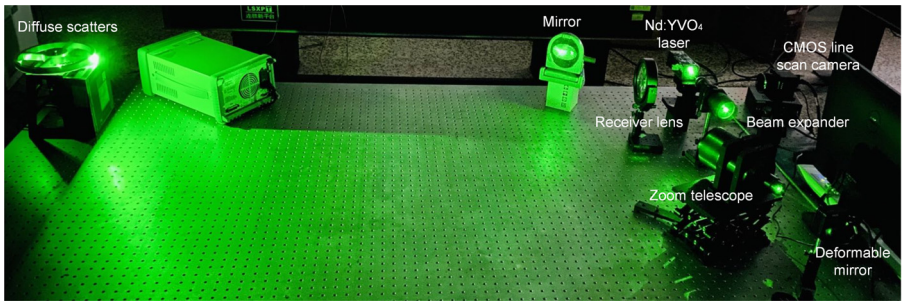

Fig. 8. Experimental setup for defining the relationship between focusing status and speckle metric.

Table 1
The speckle-averaging condition.

Speckle metric	Space scale	Time scale
J_{time}	$\Delta r_{space} > \Delta r$	$\Delta\tau < \tau_s \ll T < \tau_{at}$
J_{space}	$N_s < N_{pixels} * \Delta r_{space}/r_s$	$\Delta\tau < \tau_c$

which means the speckle metric J_{time} will be limited by the condition of target speed, that is $v > \omega/(T \cdot \tau_{at})$.

For targets with static or slowly moving surface motion, time-averaging speckle metric J_{space} can be performed by calculating the dynamic speckle spatial power spectrum. In this case, the characteristic intensity temporal correlation time τ_c can be estimated as the time required for a speckle to cross the observation point $\tau_c = r_s/v$. So the time interval $\Delta\tau$ need smaller than the life of speckle $\Delta\tau < \tau_c$, which means the frequency condition of line scan camera is $f > v\pi\omega/\lambda z$. Moreover, it is necessary to ensure that the number N_s inside non-overlapping areas of speckle spatial is sufficient. Because $N_s = N_{pixels} * \Delta r_{space}/r_s$, where $N_{pixels} * \Delta r_{space}$ is the space detection distance and $r_s = \lambda z/\pi\omega$. Therefore, the smaller target hit-spot may cause an insufficient speckle number, leading an unstable metrics J_{space}.

2.4.1. Speckle metric J_{time} based on temporal spectrum analysis

The speckle-field temporal-spectrum signals are obtained by extracting and calculating the columns of the time history of speckle pattern (THSP), as shown in Fig. 4b. In this space-averaging approach, speckle metric J_{time} is obtained by integrating multiple temporal spectrums, where N_τ is 10^3, Δr_{space} is 30 and N_{pixels} is 8. The metric J_{time} is available if the following conditions are satisfied. One is that the measurement time T is long enough to retrieve the temporal statistical properties. The other is to ensure the space interval of each temporal spectrum is larger than the maximum spatial correlation distance. The above data satisfies these time-space scales. The hit-spot size on the target surface is varied by moving the focal length f with $\Delta f = 0.12$ m. Fig. 6 shows the simulation curves of the temporal spectrum varying with the target spot size. It is clear that the bandwidth of temporal spectrum increase as the focused spot size decreases and the averaged results of the speckle metrics J_{time} have a maximum at the focal point ($f = 5$ m) corresponding to the smallest possible beam size on the target. It is verified that the speckle metric J_{time} obtained by temporal spectrum can feedback the size of the focused spot, which is consistent with the theory as Eq. (12).

2.4.2. Speckle metric J_{space} based on spatial spectrum analysis

To calculate the speckle metric J_{space} based on multiple sets of spatial spectrums, we sample 256 × 50 spatial spectrum signals by slicing the vertical axis of the THSP as shown in Fig. 4b, where N_τ is 50 and N_{pixels} is 256. This metric J_{space} can be used as a performance metric in TIL system if the following condition is fulfilled: the time interval is smaller than the lifetime of the speckle. Therefore, this metric can quickly feedback the information of the slower target hit-spot but requires a high frequency line scan camera. The simulation curves of dynamic speckle spatial spectrums are shown in Fig. 7. It is obvious that the height of the power spectrum decreases with the decrease of the target spot and the time-averaging speckle metrics J_{space} have a minimum at the focal point ($f = 5$ m) corresponding to the smallest possible beam size on the target. It validates the theoretical Eq. (7), and verifies the feasibility of the speckle metric J_{space} to monitor the focused effect of target spot, which is inversely proportional to the spot size.

3. Experiment

The scheme of experimental setup is illustrated in Fig. 8. A polarized laser beam from an Nd:YVO_4 laser ($\lambda = 0.532$ μm) is expanded to a diameter of 10 mm for filling or overfilling the pupil size of the piezoelectric deformable mirror (DM). The piezoelectric deformable mirror(from Thorlabs, Inc. DMP40 series) is comprised of a thin glass protected-silver-coated disk glued to a circular piezoelectric disk. The electrode attached to the back of the disk is divided into 40 single voltage-controlled segments arranged in a circular keystone pattern. In the experiment, let these 40 actuators work in a defocus aberration correction mode, where the physical stroke ranges from -6.5 μm to +6.5 μm when applied a 0–200 V voltage. It is used for fine-tuning focusing so that the target spot is optimally focused. Then, the light is focused onto the diffuse surface of an extended target located approximately 3.5 m from the telescope. The speckle field scattered off the diffusor is registered by the receiver system, which consists of a lens and a digital 8-bit DALSA COMS linear scan camera with a 1 × 2048 pixel resolution and 18 kHz sampling frequency.

To analyze the relationship between the spatio-temporal statistical characteristics of dynamic speckle and the target spot size, the THSP obtained by a line scan camera at different target speeds corresponding to two hit-spot sizes on the target surface is shown in Fig. 9. The first column in this figure shows that the target beam detected by beam profiler with $\omega = 1.95$ mm and $\omega = 6.12$ mm. The corresponding THSPs are arranged horizontally in this picture with a gradually increasing target speed. It is agreed with Eq. (7) and Fig. 3 that the experiment speckle size increases as the illumination area decreases. The experimental results of two metrics calculated by 500 × 2000 pixel THSP are shown in the third row of pictures. What is more, the metric J_{time} with $\Delta r_{space} = 1.4$ mm increases the accuracy (without increasing the measurement time T) by increasing the velocity of the target, due to the lifetime of dynamic speckle gradually decreases with the increase of the target speed as $\tau_c = \lambda z/\pi\omega v$. Although the speckle spatial coherence length r_s is not affected by the target speed as shown in Eq. (7), the experiment results of the metric J_{space} also gradually reduce the error as the target speed increases. Because the shorter speckle lifetime cause more statistically independent speckle pattern realizations when the measurement time T is constant. Meanwhile, a longer measurement time T will increases the accuracy of this metric when v is constant, as shown in Fig. 10.

Consider a more detailed analysis of the speckle metric's dependence on the target spot size, we control the voltage of the deformation

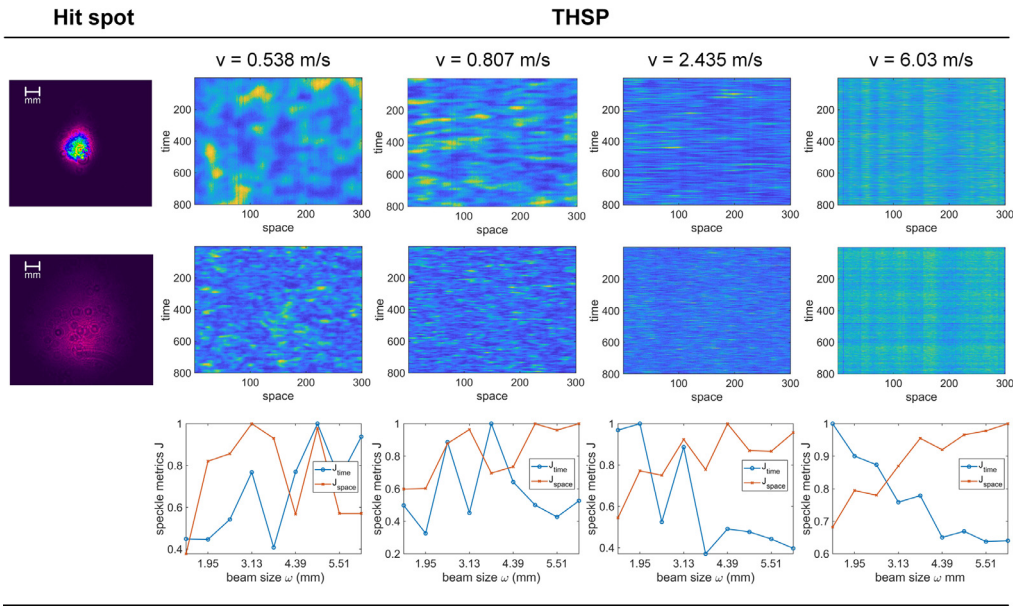

Fig. 9. The THSP obtained by a line scan camera are arranged horizontally in the picture with a gradually increasing target speed. The lifetime of dynamic speckle gradually decreases with the increase of target speed or hit-spot size, while the speckle spatial coherence length is only affected by the target hit-spot size without the speed. The metric J_{time} obtained by a 5 × 2000 pixel THSP and J_{space} obtained by a 500 × 80 pixel THSP both reduce the error as the target speed increases.

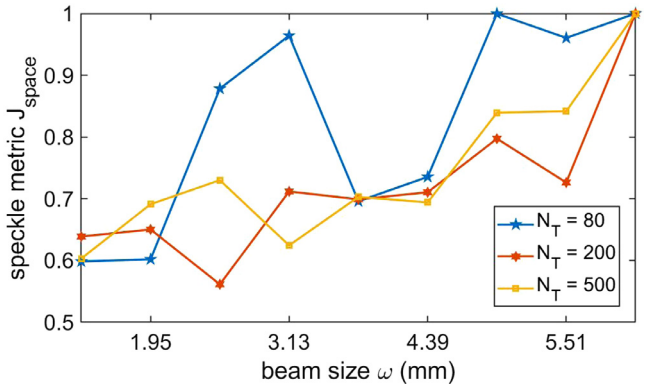

Fig. 10. The metric J_{space} with different number of sampling times N_T when $\upsilon = 0.807$ m/s.

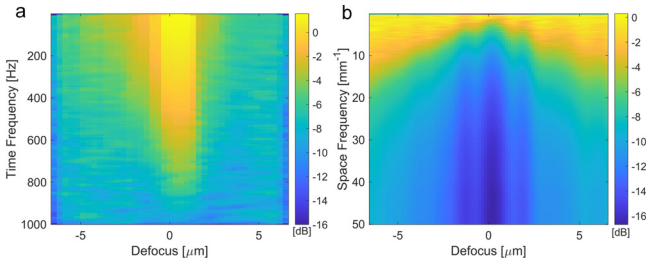

Fig. 11. The experimental results of temporal and spatial spectrum are calculated from the speckle-field intensity signals. The defocus of the DM mirror is used as a controlling parameter. And beam size on the target changed from $\omega = 5.85$ mm ($f = -6.5$ mm) to the sharply focused beam with $\omega = 0.76$ mm for f=0 mm and further to the highly defocused beam $\omega = 6.12$ mm ($f = 6.5$ mm) with the indicated control voltage change. It can be approximated as far-field for the experimental conditions due to these small spot sizes. (a) The temporal spectrum; (b) The spatial spectrum.

mirror in the experiments to obtain a continuously varying target spot size with a physical stroke interval of 0.65 μm. Table 2 describes in detail the data of two metrics obtained by speckle spectrum. And the frequency of line scan camera satisfies this time scale (18 kHz > $\upsilon\pi\omega/\lambda z$). The experimental speckle spectrum changes with the target beam size as shown in Fig. 11, which visually shows the relationship between the bandwidth frequency and the target beam size. The vertical axis represents the time-frequency spectrum of the speckle signal, note that the yellow area in each column represents the bandwidth of the spectrum. Obviously, the bandwidth frequency of temporal spectrum is maximized at the smallest possible beam size on the target surface as shown in Fig. 11a, while Fig. 11b shows the cutoff frequency of spatial spectrum is minimized at the smallest target beam size. This verifies the above conclusion. Moreover, the sharpness function boundary curve of the temporal spectrum has a better-localized extremum than the spatial spectrum corresponding to the minimum target hit-spot. Because the small target beam size more affects the speckle spatial spectrum with a short measurement time and causes a decrease in the number inside non-overlapping areas of spatial signals. However, the temporal spectrum is not always good as the boundary curve may blur when the target spot size is too large, due to the increased roughness update time and small speckle size could cause insensitivity to the detection signal.

Table 2
The time and space scales of experiment.

Speckle metric	υ (m/s)	N_{pixel}	Δr_{space} (μm)	N_τ	T (ms)	frequency (Hz)
J_{time}	6.03	50	700	1000	56	18
J_{space}	6.03	1	14	50	2.8	357

The experimental discrimination scatterplots of speckle metrics J_{time} and J_{space} obtained according to above scales are illustrated in Fig. 12. Using Eq. (13), the normalized results marked by "×" corresponding to speckle metrics J_{time} are obtained by space-averaging temporal spectrums, and the results marked by "+ " corresponding to speckle metric J_{space} are obtained by time-averaging temporal spectrums. Both metrics have their extrema (maximum for J_{time} and minimum for J_{space}) at approximately the same defocus corresponding to the smallest possible beam size on the target surface. It is no doubt that the trend of metric curves is consistent with the bandwidth boundary curve of time-frequency spectrum as Fig. 11. By comparing the data in Tab. 2, although the metric J_{time} is limited by the long measurement time and high speed of target, it is more sensitive to the small target beam

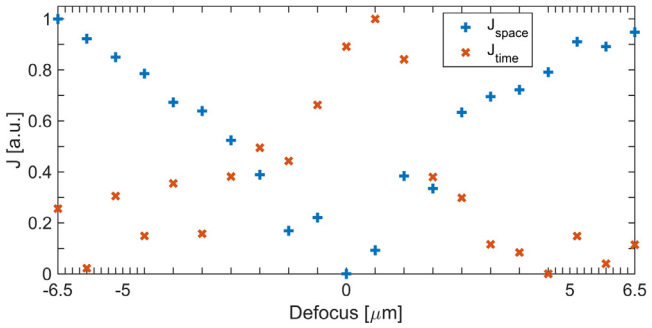

Fig. 12. The defocus position $f = 0$ corresponds to the minimum beam size on the target surface. And both metrics have their extrema (maximum for J_{time} and minimum for J_{space}) at approximately the same defocus corresponding to the smallest target beam size. And the frequency of metric J_{time} and J_{space} are 18 Hz and 357 Hz respectively.

size. On the other hand, the metric J_{space} has a high bandwidth to be applied in an adaptive TIL system, and the lack of determining the minimum target spot can be improved by increasing the measurement time. Therefore, these metrics have a monotonic dependence on the target hit-spot size. This approach of using speckle metrics to monitor the target spot can quickly determine the relative optimal value of target beam size within a certain range instead of the absolute value. What is more, the presence of well-localized extrema on the speckle metric curves that coincide with the extremum for the focused spot size is exactly the property required for adaptive control in TIL projection systems. As a result, the experiment confirms the theoretical and simulation analysis.

4. Conclusion

In this work, we have introduced the speckle formation geometry, then developed a numerical model to demonstrate the 3D Spatio-temporal characteristics of speckles, which represents the time history of the speckle pattern during the observation (THSP). Considering only the movement of the scattering center, the model reproduces reasonably well the expected first and second order spatial and temporal statistics of the dynamic speckle, which is useful to evaluate novel data analysis in dynamic speckle. Also, we provided a feasible method to feedback the beam size on the target surface by rapid estimation of the speckle-field statistical properties. This application of using line scan camera to obtain the dynamic speckle spectrum can well-balanced trade-off between sampling time and calculation accuracy. And the experimental and simulation results demonstrate that both metrics calculated in a short time have a well-localized extremum (maximum for J_{time} and minimum for J_{space}) for the smallest possible beam size on the target surface. What is more, the metric J_{space} is more suitable in an adaptive TIL system, which has a higher frequency and low requirement for target speed than J_{time}. This work provides the basis for applying dynamic speckles to monitor the variation of the beam size on the far-field target surface.

Declaration of competing interest

The authors declare that they have no known competing financial interests or personal relationships that could have appeared to influence the work reported in this paper.

Acknowledgments

This work was sponsored by National Natural Science Foundation of China (No. 61805234), Key Research Program of Frontier Science, China, CAS (No. QYZDB-SSWSLH014).

References

[1] X. Xu, X. Ren, F. Zhong, C. Quan, X. He, Optimization of speckle pattern based on integer programming method, Opt. Lasers Eng. 133 (2020) 106100.
[2] M.A. Vorontsov, Speckle effects in target-in-the-loop laser beam projection systems, Adv. Opt. Technol. 2 (5–6) (2013) 369–395.
[3] P.S. Salter, M.J. Booth, Adaptive optics in laser processing, Light Sci. Appl. 8 (1) (2019).
[4] D. Zhu, R. Wang, M. Žurauskas, P. Pande, J. Bi, Q. Yuan, L. Wang, Z. Gao, S.A. Boppart, Automated fast computational adaptive optics for optical coherence tomography based on a stochastic parallel gradient descent algorithm, Opt. Express 28 (16) (2020) 23306–23319.
[5] P. Gordo, A. Amorim, J. Abreu, F. Eisenhauer, N. Anugu, P. Garcia, O. Pfuhl, M. Haug, E. Sturm, E. Wieprecht, et al., Integration and testing of the GRAVITY infrared camera for multiple telescope optical beam analysis, in: Optical and Infrared Interferometry IV, 9146, 2014.
[6] A.K. Singh, D.N. Naik, M. Takeda, G. Pedrini, W. Osten, Exploiting scattering media for exploring 3-D objects, Light Sci. Appl. 6 (2) (2016).
[7] J.W. Goodman, Statistical Optics, John Wiley & Sons, 2015.
[8] M.A. Vorontsov, G.W. Carhart, J.W. Gowens II, Target-in-the-loop adaptive optics: wavefront control in strong speckle-modulation conditions, in: High-Resolution Wavefront Control: Methods, Devices, and Applications IV, Vol. 4825, International Society for Optics and Photonics, 2002, pp. 67–73.
[9] M. Vorontsov, T. Weyrauch, S. Lachinova, M. Gatz, G. Carhart, Speckle-metric-optimization-based adaptive optics for laser beam projection and coherent beam combining, Opt. Lett. 37 (14) (2012) 2802–2804.
[10] V.V. Dudorov, M.A. Vorontsov, V.V. Kolosov, Speckle-field propagation in "frozen" turbulence: brightness function approach, J. Opt. Soc. Amer. A 23 (8) (2006) 1924–1936.
[11] Y. Li, J. Guo, L. Liu, T. Wang, W. Tang, Z. Jiang, Clipped speckle autocorrelation metric for spot size characterization of focused beam on a diffuse target, Opt. Express 23 (6) (2015) 7424–7441.
[12] Z. Yu, J. Guo, L. Liu, T. Wang, Y. Li, Statistical properties of dynamic speckles in application to laser focusing systems, Appl. Opt. 58 (12) (2019) 3310–3316.
[13] W.J. Warren, E.A. Moro, M.E. Briggs, E.B. Flynn, Simulating translation-induced laser speckle dynamics in photon Doppler velocimetry, Appl. Opt. 53 (21) (2014) 4661–4668.
[14] D. Semenov, S. Miridonov, E. Nippolainen, A. Kamshilin, Statistical properties of dynamic speckles formed by a deflecting laser beam, Opt. Express 16 (2) (2008) 1238–1249.
[15] T. Yoshimura, Statistical properties of dynamic speckles, J. Opt. Soc. Amer. A 3 (7) (1986) 1032–1054.
[16] J. Schmidt, Numerical Simulation of Optical Wave Propagation with Examples in Matlab, in: Press Monograph, Society of Photo-Optical Instrumentation Engineers, Bellingham, 2010.
[17] E.A. Moro, M.E. Briggs, L.M. Hull, Defining parametric dependencies for the correct interpretation of speckle dynamics in photon Doppler velocimetry, Appl. Opt. 52 (36) (2013) 8661–8669.